Phospholipase A2 inhibitor and LY6/PLAUR domain-containing protein PINLYP regulates type I interferon innate immunity

Zhongshun Liu[a,1], Congwei Jiang[a,1], Zhangmengxue Lei[a,1], Sihan Dong[a,1], Linlin Kuang[a], Chenxu Huang[a], Ying Gao[a], Mu Liu[a], Hui Xiao[a], Patrick Legembre[b], Jae U. Jung[c], Huaping Liang[d], and Xiaozhen Liang[a,2]

[a]Key Laboratory of Molecular Virology & Immunology, Institut Pasteur of Shanghai, University of Chinese Academy of Sciences, Chinese Academy of Sciences, 200031 Shanghai China; [b]UMR CNRS 7276, INSERM U1262, University of Limoges, 87032 Limoges, France; [c]Department of Cancer Biology and Center for Global and Emerging Pathogen Research, Lerner Research Institute, Cleveland, OH 44106; and [d]State Key Laboratory of Trauma, Burns and Combined Injury, Department of Wound Infection and Drug, Army Medical University, 400042 Chongqing, China

Edited by Katherine Fitzgerald, University of Massachusetts Medical School, Worcester, MA; received June 16, 2021; accepted November 29, 2021

Type I interferons (IFNs) are the first frontline of the host innate immune response against invading pathogens. Herein, we characterized an unknown protein encoded by phospholipase A2 inhibitor and LY6/PLAUR domain-containing (PINLYP) gene that interacted with TBK1 and induced type I IFN in a TBK1- and IRF3-dependent manner. Loss of PINLYP impaired the activation of IRF3 and production of IFN-β induced by DNA virus, RNA virus, and various Toll-like receptor ligands in multiple cell types. Because PINLYP deficiency in mice engendered an early embryonic lethality in mice, we generated a conditional mouse in which PINLYP was depleted in dendritic cells. Mice lacking PINLYP in dendritic cells were defective in type I IFN induction and more susceptible to lethal virus infection. Thus, PINLYP is a positive regulator of type I IFN innate immunity and important for effective host defense against viral infection.

interferon | innate immunity | virus infection

Interferon (IFN)-mediated antiviral responses serve as the first line of the host innate immune defense against viral infection. IFNs are divided into three families based on sequence homology: type I, type II, and type III (1, 2). The type I IFN family encodes 13 subtypes of IFN-α in humans (14 in mice), a single IFN-β subtype, and several poorly defined subtypes (3, 4). Type I IFNs were originally identified based on their ability to interfere with viral replication, restrain virus dissemination, and activate adaptive immune responses (5–7). They can be induced in most cell types by microbial pathogen-associated and damage-associated molecular patterns recognized by pattern recognition receptors (PRRs) (3). By inducing the expression of IFN-stimulated genes (ISGs), type I IFNs elicit antiviral innate immunity and mediate adaptive immune responses (8, 9).

The induction of antiviral type I IFN response is elicited in response to the stimulation of PRRs that detect pathogen-associated molecular patterns, such as viral nucleic acids, viral replicative intermediates, and surface glycoproteins (10, 11). There are four major subfamilies of PRRs: the Toll-like receptors (TLRs), nucleotide-binding oligomerization domain/leucine-rich repeat-containing receptors, RIG-1-like receptors (RLRs), and the C-type lectin receptors, which are located at the cell surface, in the cytosol, or endosomal compartments (11–14). Among the TLR family members, TLR3, TLR7, TLR8, and TLR9 are involved in the recognition of viral nucleotides. Viral DNA enriched in CpG-DNA motifs is recognized by TLR9, single-stranded RNA is recognized by TLR7 and TLR8, and double-stranded RNA and its synthetic analog polyinosinic-polycytidylic acid (poly I:C) are recognized by TLR3 (15, 16). Some viral envelope proteins can be recognized by TLR4 or TLR2 (16, 17).

Following viral infection, cytosolic DNA can be sensed by cyclic guanosine monophosphate (GMP)–adenosine monophosphate (AMP) synthase (cGAS) that induces the production of cyclic GMP-AMP (cGAMP) (18, 19). cGAMP functions as a second messenger that binds and activates the endoplasmic reticulum (ER) adaptor STING (19–22). Translocation of activated STING from the ER to the Golgi apparatus leads to the activation of kinase TBK1, which subsequently phosphorylates IRF3 and triggers the production of type I IFN (22–24). Cytosolic RNA can be recognized by the RLRs like RIG-1 and MDA5, which signal via mitochondrial antiviral signaling protein (MAVS; also known as CARDIF, IPS1, and VISA) and subsequently activate TBK1 and IRF3–IRF7, leading to the induction of type I IFNs and other antiviral genes (25–27).

The lymphocyte antigen-6 (Ly6)/urokinase-type plasminogen activator receptor (uPAR) superfamily is characterized by the LU domain and a domain containing 10 cysteines that form distinct disulfide bridges, which create the three-fingered structural motif. The Ly6/uPAR family members regulate a wide range of functions in various cell types (28). Here, we uncovered the previously uncharacterized role of the Ly6/uPAR family member PINLYP in the induction of type I IFNs in response to DNA virus, RNA virus, and other TLR ligands. This study further defined the pivotal function of PINLYP in the effective host defense against virus infection.

Significance

Interferon (IFN)-mediated antiviral responses serve as the first line of the host innate immune defense against viral infection. Here we identify a previously uncharacterized protein designated phospholipase A2 inhibitor and LY6/PLAUR domain-containing protein (PINLYP), which is essential for embryonic development and plays an important role in type I IFN against pathogen infection. PINLYP deficiency impairs type I IFN production and dampens in vivo host defense against DNA and RNA virus infection. We unravel a unique actor in the type I IFN innate immunity and a potential target for the antiviral therapies.

Author contributions: Z. Liu, C.J., Z. Lei, P.L., J.U.J., and X.L. designed research; Z. Liu, C.J., Z. Lei, S.D., L.K., C.H., Y.G., M.L., and X.L. performed research; H.X., J.U.J., and H.L. contributed new reagents/analytic tools; Z. Liu, C.J., Z. Lei, S.D., L.K., C.H., Y.G., M.L., P.L., and X.L. analyzed data; and Z. Liu, P.L., and X.L. wrote the paper.

The authors declare no competing interest.

This article is a PNAS Direct Submission.

[1]Z. Liu, C.J., Z. Lei, and S.D. contributed equally to this work.

[2]To whom correspondence may be addressed. Email: xzliang@ips.ac.cn.

This article contains supporting information online at http://www.pnas.org/lookup/suppl/doi:10.1073/pnas.2111115119/-/DCSupplemental.

Published December 30, 2021.

Results

PINLYP Interacts with TBK1 and Activates Type I IFN. Gammaherpesvirus infection is tightly associated with lymphomas and other cancers, especially in immunodeficient hosts. Because human gammaherpesviruses only infect humans, we have previously developed a gammaherpesvirus 68 (MHV68)-associated B lymphoma mouse model for detailed investigation of the role of viral gene products and host responses in gammaherpesvirus-associated lymphomagenesis (29). To examine the gene-expression pattern between MHV68-immortalized SL-1 cells and SL-1–derived tumor cells (SL-1P) explanted from immunodeficient nude mice, Affymetrix gene-expression profiling analyses were performed and compared. The gene-expression comparison between SL-1 and SL-1P cells with the biggest fold-change is illustrated in the heatmap (*SI Appendix*, Fig. S1*A*). One of these genes was the uncharacterized phospholipase A2 inhibitor and Ly6/PLAUR domain-containing protein (PINLYP), which belongs to the Ly6/uPAR family member (*SI Appendix*, Fig. S1 *A* and *B*). The GenBank sequence indicated that mouse PINLYP encodes a 212-amino acid protein with 60% homology to its human ortholog (*SI Appendix*, Fig. S1*C*). The Human Protein Atlas pointed out that PINLYP is expressed in a broad range of tissues and does not exhibit tissue specificity (https://www.proteinatlas.org/ENSG00000234465-PINLYP). As shown in *SI Appendix*, Fig. S1*D*, PINLYP harbors a putative signal peptide at the N terminus, two conserved UPAR_Ly6 domains, and a phospholipase A2 inhibitor domain (*SI Appendix*, Fig. S1*D*).

PINLYP was significantly up-regulated in gammaherpesvirus-associated lymphoma cells and explanted tumor cells (*SI Appendix*, Fig. S1*B*) and predominantly localized in the ER of the cells, as evidenced by confocal microscopy (*SI Appendix*, Fig. S2*A*). A Flag-tagged PINLYP was transfected into 293T cells and after coimmunoprecipitation, the PINLYP interactome was analyzed by SDS/PAGE with Coomassie blue staining. One specific band exhibiting a molecular mass of above 70 kDa specifically interacted with PINLYP, whereas this protein was not detected in elution from empty vector-transfected cells (*SI Appendix*, Fig. S2*B*). Mass spectrometry analysis revealed that this 70-kDa protein corresponded to TBK1, which was originally implicated in NF-κB activation and later shown to be essential for the IRF3 signaling and IFN antiviral responses (30–33). To confirm the interaction, Flag-tagged mouse and human PINLYP were coexpressed with Myc-tagged mouse and human TBK1 in 293T cells, respectively. Coimmunoprecipitation assays confirmed that both mouse and human PINLYP interacted with TBK1 efficiently (Fig. 1*A*). Furthermore, the Flag-tagged PINLYP overexpressed in 293T cells also interacted with endogenous TBK1 (*SI Appendix*, Fig. S2*C*). Immunofluorescence experiments carried out in 293T cells cotransfected with PINLYP and TBK1 indicated that the distribution of the two markers was correlated (Pearson $r = 0.89$), suggesting that these proteins were colocalized (Fig. 1*B*). Because TBK1 plays a pivotal role in the IFN signaling pathway, we wondered whether PINLYP could contribute to this response. For this purpose, we evaluated the effect of PINLYP overexpression in an IFN reporter assay in which the luciferase expression was under the control of the IFN-β or IFN-stimulated response element (ISRE) promoter. Of note, overexpression of both human and mouse PINLYP in 293T cells activated the IFN-β and ISRE promoters (Fig. 1*C*), in a concentration-dependent manner (Fig. 1*D*). Collectively, these results established that PINLYP interacts with TBK1 and activates type I IFN responsive genes. Mouse PINLYP was used in the following experiments if not indicated specifically.

PINLYP-Mediated Type I IFN Activation Relies on Its Interaction with TBK1. The interaction between PINLYP and TBK1 prompted us to investigate whether PINLYP-mediated type I IFN activation was dependent on TBK1 and the downstream transcription factor IRF3. To test this, we generated TBK1 knockout (KO) 293T cells and IRF3 KO 293T cells using the CRISPR/Cas9 gene-editing system. Sequencing analyses confirmed the deletion of TBK1 genomic region 64460174 to 64460219 in TBK1 KO 293T cells and IRF3 genomic region 49664740 to 49664872 in IRF3 KO 293T cells. Immunoblot analyses established the deficiency of TBK1 or IRF3 expression (*SI Appendix*, Fig. S2*D*). Notably, TBK1 or IRF3 deficiency impaired the PINLYP-induced activation of IFN-β and ISRE promoters, and transfection of TBK1 or IRF3, respectively, rescued this response (*SI Appendix*, Fig. S2 *E* and *F*), suggesting that PINLYP-induced type I IFN activation is dependent on TBK1 and IRF3.

Next, to identify the PINLYP domains involved in this signal, we generated a series of AU1-tagged PINLYP deletion mutants (Fig. 1*E*). All PINLYP mutants were efficiently expressed (Fig. 1*F*). Coimmunoprecipitation revealed that the interaction was significantly weakened between TBK1 and the mutant Δ40-80, Δ150-212, or Δ180-212 (Fig. 1*F*). The PINLYP mutants Δ40-80, Δ150-212, and Δ180-212 greatly reduced the activation of the IFN-β promoter as compared to wild-type PINLYP (Fig. 1*G*). It is worth noting that the mutant Δ40-80 showed a lower expression level. To rule out the effect of expression level on the activity of PINLYP mutant, we generated the mutants Δ40-60 and Δ60-80, which were expressed at a higher level than the mutant Δ40-80 observed above (*SI Appendix*, Fig. S3 *A* and *B*). While the Δ40-60 mutant less efficiently interacted with TBK1 and triggered a reduced IFN-β signal, the Δ60-80 mutant behaved similarly to its wild-type counterpart (*SI Appendix*, Fig. S3 *A* and *B*). Immunofluorescence experiments revealed that Δ40-60 and Δ60-80 mutants were in part colocalized with TBK1, while the mutant Δ150-212 did not colocalize with TBK1 (*SI Appendix*, Fig. S3*C*). The specific interactions between PINLYP mutants and TBK1 were further clarified by the immunoprecipitation assay using 293T cells cotransfected with each PINLYP mutant with or without TBK1 (*SI Appendix*, Fig. S3*D*). These data indicated that unlike the C-terminal region 150–212, the amino acid residues 40–60 exerted a minor role in regulating the PINLYP-TBK1 interaction and the IFN-β activation. The interaction between PINLYP and TBK1 prompted us to further investigate whether PINLYP could promote the TBK1–IRF3 interaction. Coimmunoprecipitation experiments showed that PINLYP expression enhanced the intensity of the TBK1–IRF3 interaction (*SI Appendix*, Fig. S4), suggesting that PINLYP contributes to the TBK1–IRF3 interaction and subsequently enhances IRF3 activation and type I IFN production.

PINLYP Deficiency Leads to Embryonic Lethality. To decipher the biological function of PINLYP, we next generated PINLYP-deficient ($PINLYP^{-/-}$) C57BL/6J mice by using the CRISPR/Cas9 gene-editing system with the specific guide RNAs targeting PINLYP exons 1 and 2 (*SI Appendix*, Fig. S5*A*). We obtained the F0-derived F1 $PINLYP^{-92}$ mice, which carried heterozygous 92-bp deletions in the PINLYP coding region. Heterozygous $PINLYP^{-92}$ mice were interbred to obtain homozygous ($PINLYP^{-/-}$) animals. However, crosses did not produce offspring in the expected Mendelian 1:2:1 ratio because they did not yield homozygous-null pups (*SI Appendix*, Fig. S5*B*). In timed matings, PINLYP-null embryos isolated up to the embryonic day (E) 10.5 appeared alive and normal, whereas those isolated at E11.5 and E13.5 were dead (*SI Appendix*, Fig. S5 *C* and *D*), suggesting that PINLYP deficiency leads to an early embryonic lethality. $PINLYP^{-92}$ heterozygous mice were inbred and mouse embryonic fibroblasts (MEFs) were isolated from embryos at E10.5 and genotyped by PCR amplification (*SI Appendix*, Fig. S5*E*). Wild-type and homozygous KO MEFs

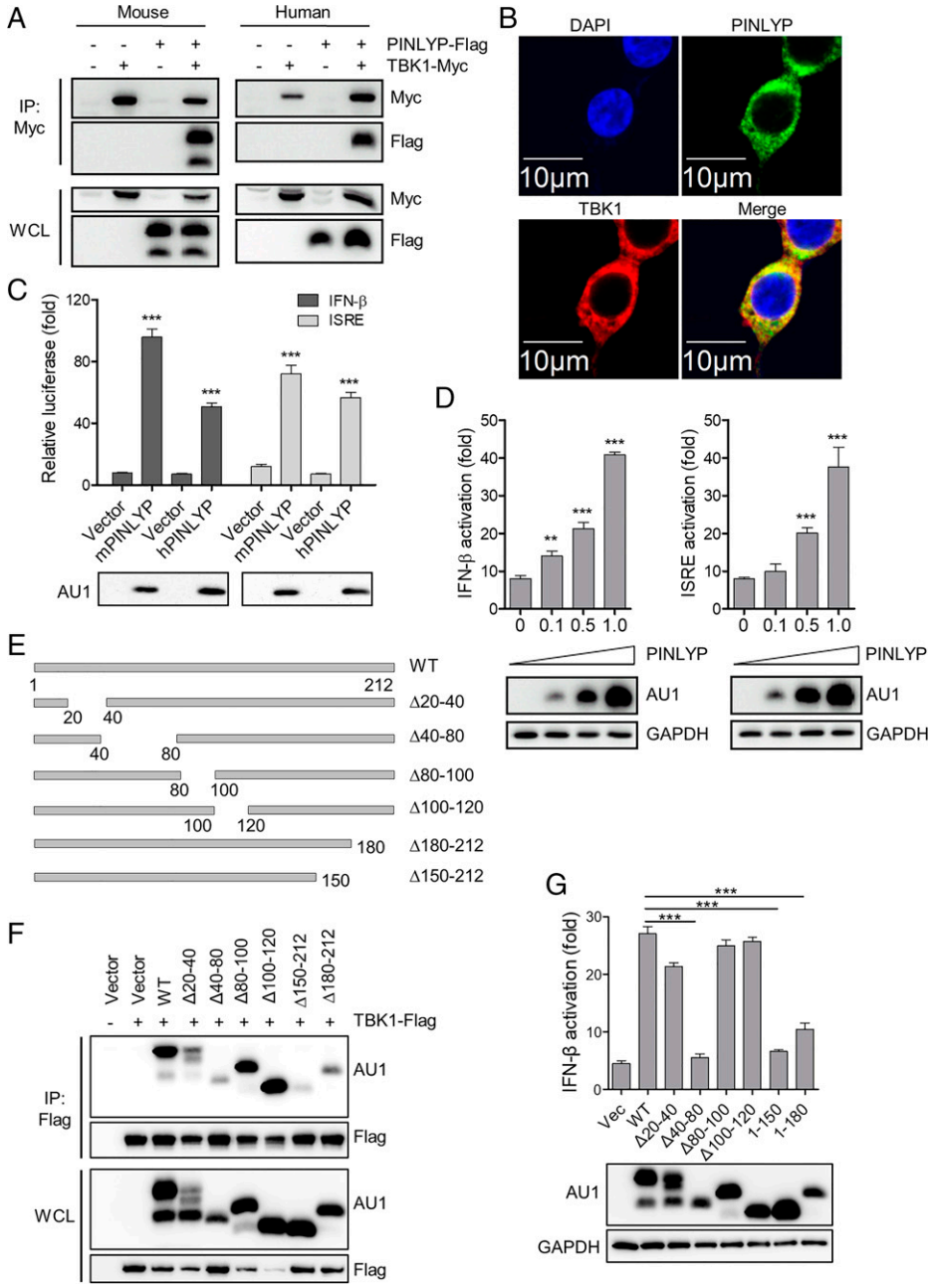

Fig. 1. PINLYP activates type I IFN through interaction with TBK1. (*A*) Whole cell lysates (WCL) were prepared from 293T cells transfected with indicated plasmids encoded by mouse or human for 48 h, immunoprecipitated with Myc-agarose, and analyzed by immunoblotting with specific antibodies as indicated. (*B*) 293T cells were transfected with PINLYP-Flag and TBK1-Myc plasmids for 48 h, fixed, and stained with Flag (green) and Myc (red) antibodies. The nucleus was stained with DAPI. (*C*) 293T cells were transfected with mouse PINLYP (mPINLYP) or human PINLYP (hPINLYP) expressing plasmids with the AU1 tag, together with IFN-β or ISRE luciferase reporter, as well as *Renilla* reporter as an internal control. At 48 h posttransfection, luciferase activity was measured and normalized to *Renilla* activity. PINLYP expression was detected by immunoblotting with the AU1 antibody. (*D*) Similar to *C*, except that increasing amounts of mPINLYP-AU1 expression plasmid were transfected into 293T cells. (*E*) Schematic diagram of mPINLYP-AU1 deletion mutants. (*F*) 293T cells were transfected with TBK1-Flag, together with mPINLYP-AU1 or the indicated deletion mutants for 48 h. TBK1-Flag immunoprecipitates and corresponding WCL were immunoblotted with Flag and AU1 antibodies. (*G*) 293T cells were transfected with mPINLYP-AU1 or the indicated deletion mutants, together with IFN-β reporter as well as *Renilla* reporter as an internal control. At 48 h posttransfection, luciferase activity was measured and normalized to *Renilla* activity. mPINLYP and mutants were detected by immunoblotting with the AU1 antibody. All error bars indicate SEM, $^{**}P < 0.01$, $^{***}P < 0.001$, two-tailed unpaired *t* test.

were immortalized by transduction with retroviruses expressing human papillomavirus (HPV)16 E6 and E7 proteins and subsequently used for further experiments. PINLYP deficiency was confirmed by immunoblot analyses (*SI Appendix*, Fig. S5*F*). These findings indicated that PINLYP possessed critical functions in embryonic development.

PINLYP Deficiency Prevents Type I IFN Induction in MEFs. We next exposed the immortalized wild-type or PINLYP KO MEFs to DNA virus herpes simplex virus-1 (HSV-1) and RNA virus vesicular stomatitis virus (VSV) to further investigate the PINLYP-mediated type I IFN responses. PINLYP^{-92} MEFs underwent a significant decrease in the production of IFN-β

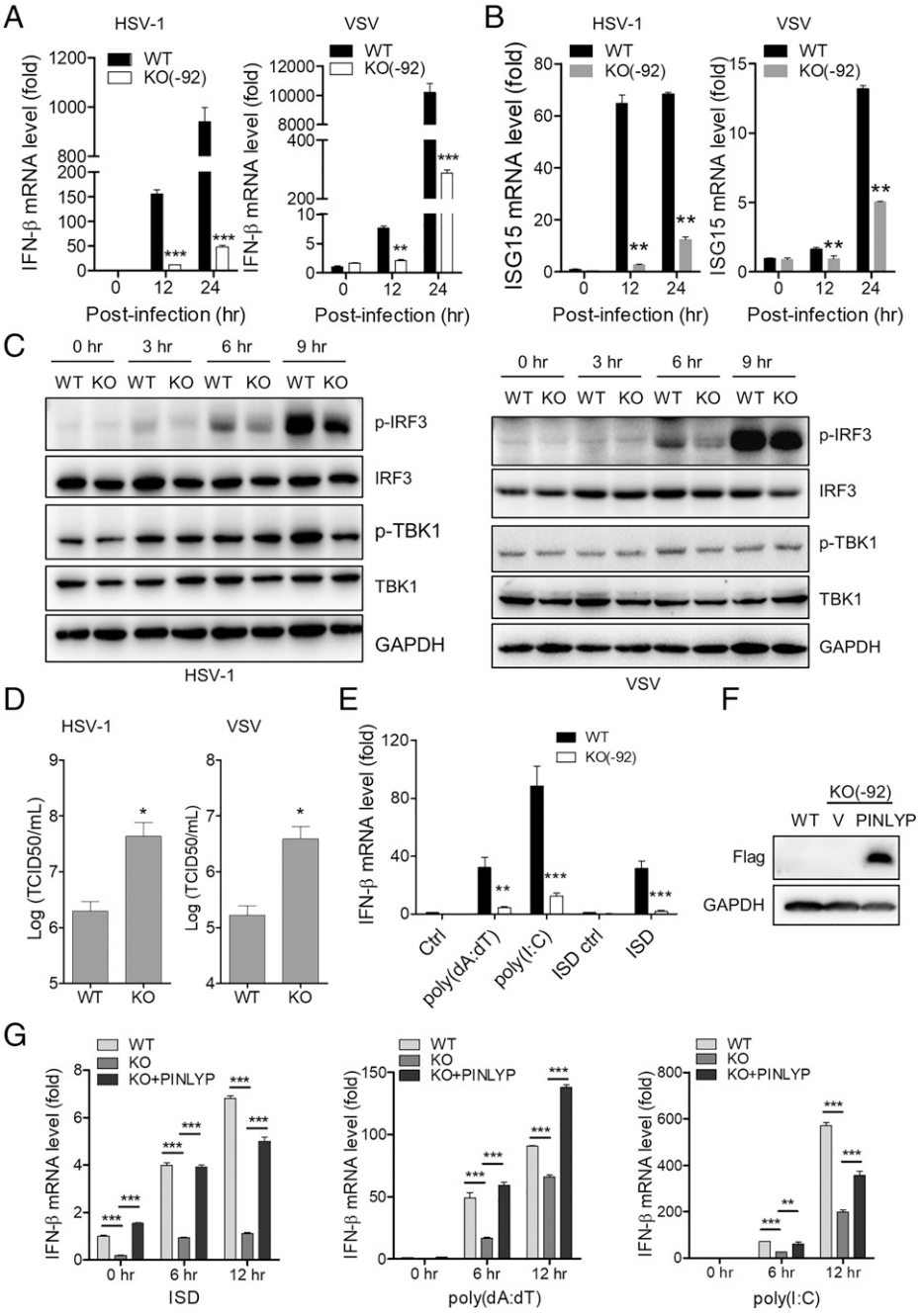

Fig. 2. PINLYP is important for type I IFN production in MEFs. (*A*) Immortalized PINLYP^{-92} MEFs were infected with HSV-1 at a multiplicity of infection (MOI) of 0.1 or VSV at an MOI of 0.01 for the indicated time, and IFN-β mRNA was measured and normalized to GAPDH mRNA. (*B*) Same experiment as *A*, except that ISG15 mRNA was measured and normalized to GAPDH mRNA. (*C*) Immortalized PINLYP^{-92} KO MEFs were infected with HSV-1 or VSV at an MOI of 10 for the indicated time; WCL were prepared and subjected to immunoblotting analyses with the indicated antibodies. (*D*) Immortalized PINLYP^{-92} KO MEFs were infected with HSV-1 at an MOI of 0.1 or VSV at an MOI of 0.01 for 24 h. The supernatant was harvested for $TCID_{50}$ titering assay. (*E*) Immortalized PINLYP^{-92} KO MEFs were treated with 0.1 μg/mL poly(dA:dT), 0.5 μg/mL poly(I:C), 1 μg/mL ISD or control (ctrl) for 8 h, IFN-β mRNA was measured and normalized to GAPDH mRNA. (*F*) Immortalized PINLYP^{-92} KO MEFs were transduced with lentiviruses expressing vector (V) or PINLYP-Flag for 48 h; WCL were prepared and subjected to immunoblotting analyses with the indicated antibodies. WT represents immortalized wild-type MEFs. (*G*) Immortalized wild-type MEFs, PINLYP^{-92} KO MEFs, or PINLYP^{-92} KO MEFs transduced with PINLYP-Flag–expressing lentiviruses for 48 h were treated with 1 μg/mL ISD, 0.1 μg/mL poly(dA:dT), or 0.5 μg/mL poly(I:C) for the indicated time; IFN-β mRNA was measured by qRT-PCR and normalized to GAPDH mRNA. All error bars indicate SEM, $*P < 0.05$, $**P < 0.01$, $***P < 0.001$, two-tailed unpaired *t* test.

mRNA as compared to that in their wild-type counterparts when the cells were challenged with HSV-1 or VSV infection (Fig. 2*A*). In agreement with these findings, the expression level of ISG15 mRNA was reduced in PINLYP^{-92} KO MEFs as compared to that in wild-type MEFs at 12 and 24 h after HSV-1 and VSV infection (Fig. 2*B*). Furthermore, PINLYP deficiency resulted in a reduction in the phosphorylation of IRF3 at Ser396 after HSV-1 and VSV infection (Fig. 2*C*), a pivotal step in the CREB-binding protein (CBP)/p300 binding and transcription activation (34). PINLYP KO also

markedly increased infection by both HSV-1 and VSV viruses, as determined by virus titer assays (Fig. 2*D*), indicating that PINLYP was important for the induction of IFN-β and immune defense against viral infection.

Because intracellular DNA from pathogens and cytosolic double-stranded RNA produced by most viruses could be recognized by multiple PRRs, we next examined the role of PINLYP in the activation of type I IFN induced by interferon stimulatory DNA (ISD), which is a cytosolic DNA sensor agonist, synthetic double-stranded DNA analog poly(dA:dT), and synthetic double-stranded RNA analog poly(I:C). Induction of IFN-β mRNA was significantly reduced in PINLYP^{-92} KO MEFs after ISD, poly(dA:dT), and poly(I:C) stimulation (Fig. 2*E*), whereas restoration of PINLYP expression in PINLYP^{-92} KO MEFs rescued the expression of IFN-β mRNA induced by ISD, poly(dA:dT), and poly(I:C) (Fig. 2 *F* and *G*). In addition, overexpression of different PINLYP constructs in PINLYP^{-92} KO MEFs showed that the Δ150-212 mutant exhibiting lower TBK1 interaction and IFN-β activation as compared to their wild-type counterpart (Fig. 1 *F* and *G*), significantly impaired IFN-β mRNA expression as compared to the wild-type PINLYP in response to poly(dA:dT) (*SI Appendix*, Fig. S6). Notably, the Δ40-60 mutant displayed a lower level of IFN-β expression than the wild-type PINLYP and the Δ60-80 mutant (*SI Appendix*, Fig. S6). Collectively, these data highlighted that PINLYP was critical for IFN-β induction by virus infection as well as cytosolic DNA and RNA stimulation.

PINLYP Deficiency Inhibits Type I IFN Production in Antigen-Presenting Cells. Because plasmacytoid dendritic cells (DCs) are the main producer of IFN and myeloid lineage cells also contribute to this response, we next generated loxp-flanked PINLYP animals (PINLYP$^{fl/fl}$) that were bred with mice expressing Cre recombinase under the control of the CD11c promoter (CD11c Cre) or lysozyme promoter (LysM Cre) (*SI Appendix*, Fig. S5*G*). FACS analyses showed the comparable CD11c^{+} cell populations in the lungs, spleens, and peritoneal cavities, as

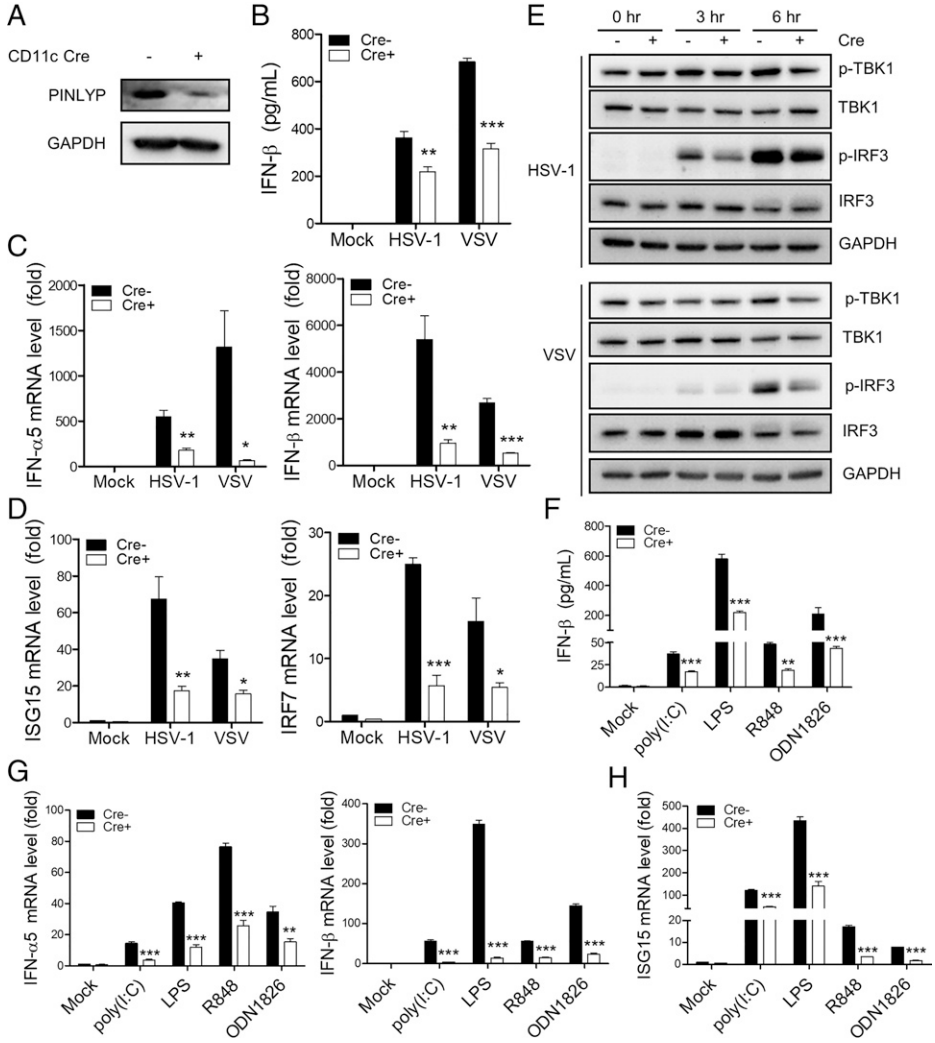

Fig. 3. PINLYP is important for type I IFN production in BMDCs. (*A*) BMDCs were prepared from PINLYP$^{fl/fl}$CD11c Cre^{-} and Cre^{+} mice. PINLYP expression was detected by immunoblot analyses in Cre^{-} and Cre^{+} BMDCs. (*B*) Cre^{-} and Cre^{+} BMDCs were infected with HSV-1 or VSV (MOI = 1) for 24 h, and supernatant IFN-β level was measured by ELISA. (*C*) Cre^{-} and Cre^{+} BMDCs were infected with HSV-1 or VSV (MOI = 1) for 4 h, IFN-α5 and IFN-β mRNA was measured by qRT-PCR and normalized to GAPDH mRNA. (*D*) Same experiment as *C*, except that ISG15 and IRF7 mRNA was measured by qRT-PCR and normalized to GAPDH mRNA. (*E*) Cre^{-} and Cre^{+} BMDCs were infected with HSV-1 or VSV (MOI = 1) for the indicated time point, followed by immunoblot analyses with the indicated antibodies. (*F*) Cre^{-} and Cre^{+} BMDCs were treated with 25 μg/mL poly(I:C), 2 μg/mL LPS, 2.5 μM R848, or 2 μM ODN1826 for 24 h, supernatant IFN-β level was measured by ELISA. (*G–H*) Cre^{-} and Cre^{+} BMDCs were treated with 25 μg/mL poly(I:C), 2 μg/mL LPS, 2.5 μM R848, or 2 μM ODN1826 for 4 h; IFN-α5 and IFN-β mRNA (*G*) or ISG15 mRNA (*H*) was measured by qRT-PCR and normalized to GAPDH mRNA. All error bars indicate SEM, $*P < 0.05$, $**P < 0.01$, $***P < 0.001$, two-tailed unpaired *t* test.

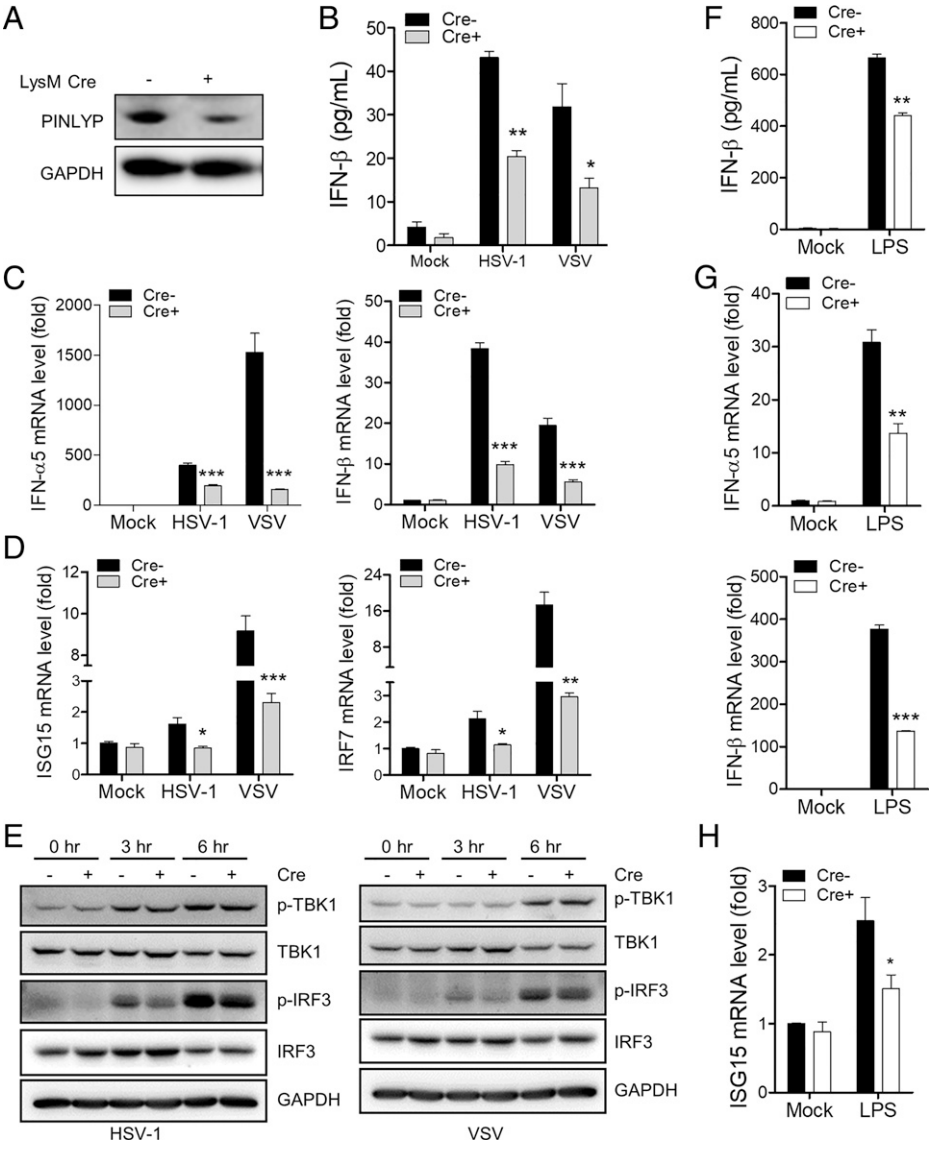

Fig. 4. PINLYP is important for type I IFN production in BMDMs. (*A*) BMDMs were prepared from PINLYP$^{fl/fl}$LysM Cre^{-} and Cre^{+} mice. PINLYP expression was detected by immunoblot analyses in Cre^{-} and Cre^{+} BMDMs. (*B*) Cre^{-} and Cre^{+} BMDMs were infected with HSV-1 or VSV (MOI = 10) for 24 h, supernatant IFN-β level was measured by ELISA. (*C*) Cre^{-} and Cre^{+} BMDMs were infected with HSV-1 or VSV (MOI = 10) for 4 h, IFN-α5 and IFN-β mRNA was measured by qRT-PCR and normalized to GAPDH mRNA. (*D*) Same experiment as *C*, except that ISG15 and IRF7 mRNA was measured by qRT-PCR and normalized to GAPDH mRNA. (*E*) Cre^{-} and Cre^{+} BMDMs were infected with HSV-1 or VSV (MOI = 10) for the indicated time point, followed by immunoblot analyses with the indicated antibodies. (*F*) Cre^{-} and Cre^{+} BMDMs were treated with 1 μg/mL LPS for 24 h, supernatant IFN-β level was measured by ELISA. (*G* and *H*) Cre^{-} and Cre^{+} BMDMs were treated with 1 μg/mL LPS for 4 h; IFN-α5 and IFN-β mRNA (*G*), or ISG15 mRNA (*H*) was measured by qRT-PCR and normalized to GAPDH mRNA. All error bars indicate SEM, $*P < 0.05$, $**P < 0.01$, $***P < 0.001$, two-tailed unpaired *t* test.

well as comparable splenic plasmacytoid DCs between PINLYP$^{fl/fl}$CD11c Cre^{-} and Cre^{+} mice (*SI Appendix*, Fig. S5 *H* and *I*), indicating that PINLYP deficiency did not affect dendritic cell development. Bone marrow-derived dendritic cells (BMDCs) generated from PINLYP$^{fl/fl}$CD11c Cre^{-} or Cre^{+} mice were isolated and immunoblot analyses confirmed the loss of PINLYP in PINLYP$^{fl/fl}$CD11c Cre^{+} BMDCs (Fig. 3*A*). The level of secreted IFN-β was significantly lower in PINLYP$^{fl/fl}$CD11c Cre^{+} BMDCs than in Cre^{-} BMDCs after exposure to HSV-1 or VSV viruses (Fig. 3*B*). The expression of IFN-α and IFN-β mRNAs in PINLYP-KO BMDCs was dramatically reduced as compared to those in control BMDCs (Fig. 3*C*). Similarly, the expression of ISG15 and IRF7 was also affected in PINLYP-deficient BMDCs (Fig. 3*D*). Consistent with the reduction of type I IFNs, PINLYP-deficient BMDCs exhibited diminished activation of IRF3 in response to HSV-1 and VSV infection, as observed by the decreased phosphorylation of IRF3 at S396 in PINLYP-deficient BMDCs (Fig. 3*E*). We next examined the expression of type I IFN and ISGs induced by various TLR ligands. PINLYP-deficient BMDCs were defective in their ability to secrete IFN-β (Fig. 3*F*) and to induce IFN-α, IFN-β, and ISG15 mRNA expression when exposed to poly(I:C), LPS, R848, and ODN1826 (Fig. 3 *G* and *H*). These results established that PINLYP plays a pivotal role in the virus- and TLR-induced type I IFN responses in DCs.

Finally, we wondered whether PINLYP would also play an important role in type I IFN activation in macrophages. To address this question, bone marrow-derived macrophages (BMDMs) were generated from PINLYP$^{fl/fl}$LysM Cre^{-} or Cre^{+} mice. PINLYP KO efficiency was determined and confirmed by

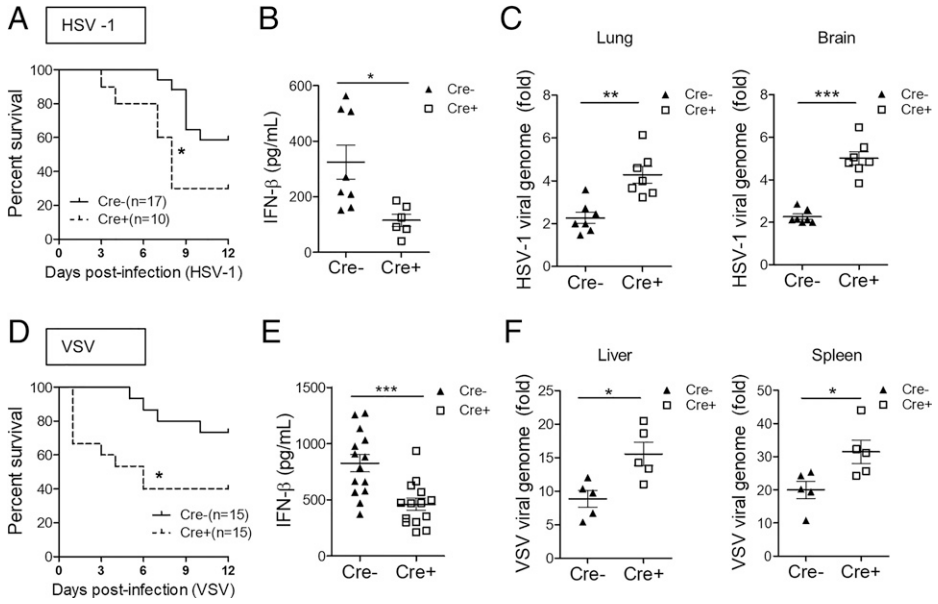

Fig. 5. PINLYP is important for effective in vivo host defense. (*A*) PINLYP$^{fl/fl}$CD11c Cre^{-} and Cre^{+} mice were infected with HSV-1 (1×10^8 pfu) via tail vein injection and survival was monitored. (*B*) Serum from PINLYP$^{fl/fl}$CD11c Cre^{-} and Cre^{+} mice were analyzed for IFN-β production by ELISA after 8 h infection with HSV-1 (1×10^8 pfu) via tail vein injection. (*C*) PINLYP$^{fl/fl}$CD11c Cre^{-} and Cre^{+} mice were infected with HSV-1 (1×10^8 pfu) via tail vein injection, and lungs and brains were retrieved for HSV-1 genome copy quantitation at day 3 postinfection. (*D*) PINLYP$^{fl/fl}$CD11c Cre-$^{-}$and Cre^{+} mice were infected with VSV (5×10^8 pfu) via tail vein injection and survival was monitored. (*E*) Serum from PINLYP$^{fl/fl}$CD11c Cre^{-} and Cre^{+} mice were analyzed for IFN-β production by ELISA after 6 h infection with VSV (5×10^8 pfu) via tail vein injection. (*F*) PINLYP CD11c Cre^{-} and Cre^{+} mice were infected with VSV (5×10^8 pfu) via tail vein injection; livers and spleens were retrieved for VSV genome copy quantitation at day 3 postinfection. The survival curve was generated by Kaplan–Meier methods and followed by log-rank test analysis. Unpaired *t* test indication: $*P < 0.05$, $**P < 0.01$, $***P < 0.001$.

immunoblot analyses (Fig. 4*A*). In responses to HSV-1 and VSV infection, PINLYP-deficient macrophages displayed a reduction of IFN-β secretion (Fig. 4*B*), a decrease in IFN-α, IFN-β, ISG15, and IRF7 mRNA expression (Fig. 4 *C* and *D*), and a weakened activation of IRF3 (Fig. 4*E*) as compared to those observed in wild-type cells. Similar results were obtained in response to LPS stimulation (Fig. 4 *F–H*), suggesting that PINLYP was a major factor for the virus- and TLR-induced type I IFN responses in macrophages.

PINLYP Is Important for Effective In Vivo Host Defense. We next investigated whether the loss of PINLYP in antigen-presenting cells could affect the antiviral response. Using PINLYP$^{fl/fl}$CD11c Cre^{-} or Cre^{+} mice infected intravenously with the DNA virus HSV-1, we observed that PINLYP$^{fl/fl}$CD11c Cre^{+} mice were more sensitive to HSV-1 lethal infection compared to Cre^{-} control mice (Fig. 5*A*). Analysis of sera from PINLYP$^{fl/fl}$CD11c Cre^{+} mice revealed a defect in the IFN-β production at 8 h after HSV-1 infection as compared to Cre^{-} control mice (Fig. 5*B*). The reduced induction of IFN-β coincided with a higher viral genome copy of HSV-1 in the lungs and brains of infected PINLYP$^{fl/fl}$ CD11c Cre^{+} mice as compared to Cre^{-} mice (Fig. 5*C*). Similarly, VSV (i.e., RNA virus) infection was more lethal in PINLYP$^{fl/fl}$CD11c Cre^{+} mice as compared to that observed in control counterpart (Cre^{-}) (Fig. 5*D*) and the lower serum level of IFN-β dosed in PINLYP-deficient mice compared to that in control animals (Fig. 5*E*) was associated with a higher number of VSV genome copies in the livers and spleens of PINLYP$^{fl/fl}$CD11c Cre^{+} mice (Fig. 5*F*). Overall, these findings established that PINLYP expression in DCs is pivotal to exert an efficient antiviral response against RNA and DNA viruses.

Discussion

PINLYP is a member of the Ly6/uPAR superfamily of proteins, characterized by a conserved domain of ∼100 amino acids containing 10 cysteine residues involved in 5 disulfide bonds (28, 35, 36). To date, 35 human and 61 mouse proteins belong to the Ly6/uPAR family, and their expression patterns and functions vary across a wide range of cell types and tissues (37–41). This protein family contributes to different physiologic processes, including inflammation, complement activity, angiogenesis, wound healing, and cancer growth (28, 39). This study reveals that PINLYP plays a pivotal role in embryonic development and in the type I IFN-mediated innate immunity.

Ly6/uPAR family members are usually subdivided into membrane-tethered or secreted groups based on the presence or absence of the glycosylphosphatidylinositol (GPI)-anchor domain (28). Although PINLYP has a predicted signal peptide in the N terminus and lacks a GPI-anchor signal in the C terminus, this protein seems to mainly reside in the ER. TBK1 is the central kinase of type I IFN signaling and its activity and cellular localization are regulated by different interacting partners including STING (20, 42–44). We show that PINLYP colocalizes with TBK1 in the cytosol and interacts with the kinase, but whether PINLYP could regulate TBK1 subcellular localization like STING remains to be elucidated and needs further investigation. Because of the putative signal peptide, we cannot rule out that a secreted form of PINLYP exists and whether this secreted form is internalized by a yet unknown receptor. This hypothesis will be explored in the future.

The function of Ly6/uPAR proteins in viral infection remains poorly studied, only a few of them are involved in viral pathogenesis—such as Ly6E, uPAR, and CD59—which are associated with the regulation of HIV-1 infection (45). Because PINLYP is up-regulated in gammaherpesvirus-associated lymphoma cells, it would be interesting to further investigate the biological role of this protein in gammaherpesvirus infection and in lymphomagenesis. The expression of some Ly6/uPAR family members can be regulated by IFN and viral infection (45); how PINLYP expression is modulated in response to different viral infections is under investigation.

In recent years, how viruses trigger innate immune responses has been extensively studied. The pathways of type I IFN production and receptor signaling have been progressively delineated, especially for cGAS-STING-TBK1–mediated type I IFN by DNA viruses and RIG-1-MAVS-TBK1–mediated type I IFN by RNA viruses (1, 3, 26). To study the biological role of PINLYP, we generated PINLYP-deficient mice that died around E11.5, highlighting the role of PINLYP in embryonic development. On the other hand, PINLYP$^{fl/fl}$ CD11c^{+} mice exhibiting a loss of PINLYP in DCs experience normal development and these animals reveal that PINLYP is responsible for triggering the type I IFN response in DCs exposed to DNA and RNA viruses. It has been reported that HSV-1 infection activates multiple mechanisms of pathogen recognition, which operate in cell-type– and time-dependent manners to trigger expression of type I IFN and coordinate the antiviral response (46). Our data revealed that PINLYP is important for type I IFN production in DCs and macrophages in response to HSV-1 and VSV infections. From a molecular standpoint, PINLYP fails to activate the IFN-α and IFN-β promoters in cells deficient in TBK1 or IRF3 and PINLYP contributes to the TBK1–IRF3 interaction. The reduction of IRF3 phosphorylation is not very robust as compared to the reduction of IFN-β production in PINLYP-deficient cells. We reason that PINLYP might have other functions that play a part in promoting IFN-β production. It is worth noting that a modest amount of TBK1 phosphorylation is detected in both wild-type and PINLYP-deficient cells in our baseline conditions, which might be attributed to the cell conditions of immortalized MEFs and bone marrow-derived and induced cells. Based on this study, we hypothesize that PINLYP is an adaptor protein promoting the TBK1–IRF3 interaction and subsequent type I IFN production. Additional studies are required to elucidate this mechanism in more detail. In conclusion, our data unravel a unique actor in the type I IFN response and suggest that PINLYP could represent a novel target for the stimulation of antiviral responses.

Materials and Methods

Cell Culture. The 293T, 293FT, HPV-16 E6/E7 packaging cell line PA317/LXSN/16E6E7 (provided by J.U.J.) and immortalized MEFs were cultured in DMEM (Gibco) supplemented with 10% heat-inactivated FBS (Gibco), 200 IU/mL penicillin, and 100 μg/mL streptomycin. SL-1 and SL-1P B cells were cultured in RPMI1640 (Gibco) supplemented with 5% heat-inactivated FBS, 200 IU/mL penicillin, and 100 μg/mL streptomycin.

MEFs were prepared from the individual embryo of heterozygous mice at day E10.5 following the protocol as previously described (47) and subjected to genotyping. Wild-type and PINLYP homozygous KO MEFs were immortalized by the retroviruses expressing HPV-16 E6 and E7, which were produced from the packaging cell line PA317/LXSN/16E6E7. Murine primary B cells were isolated from C57BL/6 mice using EasySep Mouse B Cell isolation kit (19854, StemCell) following the manufacturer's instruction.

BMDMs and BMDCs were generated as previously described (48). Briefly, bone marrow cells from murine tibias and femurs were passed through a nylon mesh to remove debris. For BMDC, bone marrow cells were cultured in RPMI 1640 supplemented with 10% FBS, 1% MEM nonessential amino acids, 1% penicillin/streptomycin, 1 mM sodium pyruvate, and 20 ng/mL mouse granulocyte-macrophage colony-stimulating factor (GM-CSF). The nonadherent cells were collected on day 7. For BMDM, bone marrow cells were cultured in DMEM supplemented with 20% supernatant taken from L929 cell culture, 10% FBS, 1% MEM nonessential amino acids, 1% penicillin/streptomycin, 1 mM sodium pyruvate, and 5 ng/mL mouse M-SCF. The adherent cells were collected on day 6.

Generation of Deficient Mice. PINLYP-deficient mice were generated in the C57BL/6 background using the CRISPR/Cas9 gene-editing system by Shanghai Biomodel Organism Science & Technology Development Co. The PINLYP single-guide RNA sequences were targeted at exon1 (TAGAAGACACAGGACCTTCC) and exon 2 (GGTGTGCAAAGGCTCGGGGCA). Homozygous, heterozygous, and WT mice were genotyped with the specific primers (forward: 5′-TTGGGAAAGGAGAAGAGGAT-3′; reverse: 5′-GGTAACCAGAAGAGGGCATAA-3′).

PINLYP$^{fl/fl}$ mice were generated by Beijing Biocytogen Co. Briefly, targeting of murine PINLYP was performed by flanking exons 2 and 5 with the LoxP sites by homologous recombination in C57BL/6 embryonic stem (ES) cells. G418-resistant clones were screened by PCR for homologous recombination at both homology arms. Chimeric mice with floxed PINLYP alleles were generated by blastocyst injection of heterozygous PINLYP$^{fl/+}$ ES cell clones. Founder PINLYP$^{fl/+}$ mice were bred with Flp-deleter mice (Biocytogen) to remove the neomycin resistance gene cassette. PINLYP$^{fl/fl}$ mice were bred with CD11C-cre mice (provided by H.X.) to generate DC-specific deletion of PINLYP, or bred with Lyz2-cre mice (provided by Guangxun Meng, Institut Pasteur of Shanghai, Shanghai, China) to generate myeloid-specific deletion of PINLYP.

All mice were maintained in pathogen-free facilities and used in accordance with the protocol (A2020061) approved by the Institutional Animal Care and Use Committee at Institut Pasteur of Shanghai.

Plasmids. The PINLYP and TBK1 coding regions were amplified from 293T cells or SL-1 cells, and subsequently cloned into the vector pLVX-puromycin (kindly provided by Jing Zhong, Institut Pasteur of Shanghai, Shanghai, China) with the C-terminal Flag, AU1, or Myc tag to yield the plasmids hPINLYP-AU1, hPINLYP-Flag, mPINLYP-AU1, mPINLYP-Flag, hTBK1-Myc, mTBK1-flag, mTBK1-Myc. The specific primers used are shown in *SI Appendix*, Table S1. TBK1 and IRF3 KO plasmids, lentiCRISPRv2-TBK1 and lentiCRISPRv2-IRF3, were generated with the lentiviral CRISPR/Cas9 system. The sgRNAs targeting TBK1 and IRF3 were cloned into a lentiCRISPRv2 vector (Addgene) following the protocols provided by Addgene using the specific targeting sequences as shown in *SI Appendix*, Table S1.

Reagents. The TLR ligands ISD (tlrl-isdc), ISD control (tlrl-isdcc), poly (I:C) (tlrl-piclv), and poly(dA:dT) (tlrl-patc) were from InvivoGen. Recombinant mouse GM-CSF (415-ML) and mouse M-CSF (416-ML) were from R&D Systems. LPS (L4391), collagenase (C5138), and 3× Flag peptide (F4799) were from Sigma-Aldrich.

The polyclonal antibodies of mPINLYP were produced using two New Zealand White rabbits immunized with the purified mPINLYP protein by Applied Protein Technology (Shanghai). mPINLYP cDNA amplified from SL-1 cells (29) was cloned into pET21 vector with a His-tag, which was subsequently transformed into BL21 competent cells. After isopropyl-β-D-thiogalactopyranoside induction of mPINLYP expression and cell lysates were prepared, mPINLYP protein was purified using Ni-NTA agarose (Qiagen) according to the manufacturer's instructions and used for immunization of White rabbits. Other antibodies are described in *SI Appendix*, Table S2.

Lentivirus Transduction and Generation of KO Cell Lines. To produce lentiviruses, 293FT cells were transfected with the lentiviral expression plasmids and packaging plasmids pMD2.G and psPAX2 (provided by Jin Zhong, Institut Pasteur of Shanghai, Shanghai, China) using the Tenfect reagent (TEYE) according to the manufacturer's instructions. The lentiviruses in the culture supernatant were collected at 48 and 72 h posttransfection, mixed with polybrene (8 μg/mL), and used for lentiviral transduction of MEFs by spinoculation at 2,000 rpm for 1 h.

To generate TBK1 or IRF3 KO cell lines, 293T cells were transfected with 4 μg lentiCRISPRv2-vector, lentiCRISPRv2-TBK1, or lentiCRISPRv2-IRF3 using the Tenfect reagent (TEYE). After 48-h transfection, the transfected cells were selected with puromycin at a concentration of 2 μg/mL for 2 wk and subsequently cloned by limiting dilution culture. Individual clones were subjected to sequencing analyses to confirm the deletion of the targeted genome region and immunoblot analyses to detect KO efficiency.

Immunoprecipitation and Mass Spectrometry. For immunoprecipitation, transfected cells or stimulated cells were lysed with RIPA buffer (50 mM Tris·HCl, PH 7.4, 150 mM NaCl, 0.1% SDS, 10 mM EDTA, 1% Triton X-100) supplemented with the protease inhibitor complete tablet (Roche). After cell lysates were centrifuged at 12,000 rpm for 15 min, the supernatant was precleared with protein A/G agarose (Thermo Scientific) and immunoprecipitated with the specific antibody-conjugated affinity gels, or specific antibody plus protein A/G agarose. Immunoprecipitates were analyzed by immunoblot analyses.

For mass spectrometry, 10 10-cm plates of 293T cells were transfected with vector or pLVX/mPINLYP-Flag expression plasmids. Cells harvested at 48 h posttransfection were lysed with 5 mL RIPA buffer supplemented with protease inhibitor complete tablet (Roche) and subjected to immunoprecipitation with anti-Flag M2 affinity gel (Sigma). The immunoprecipitates were eluted with 100 μL of 200 μg/mL 3× Flag peptide, separated on the 12% SDS/PAGE gel, and stained with Coomassie blue. The specific bands were sliced for mass spectrometry analyses by PSI Biosciences.

Affymetrix Gene-Expression Profiling Analysis. Total RNA was isolated from SL-1 cells and subjected to gene-expression profiling analyses using Affymetrix GeneChip Mouse Genome 430 2.0 Array (performed and analyzed by LC Sciences). All data were normalized using the RNA expression statistical analysis (Robust Multiarray Analysis). They were the log-scale normalized intensities from the chip (log_2 scale). In an ANOVA test, linear models were fitted to allow comparison of expression levels of different groups of replicates. The *P* value cutoff was set to 0.05. The sorted fold-change data of the comparisons are shown in the heatmap (*SI Appendix*, Fig. S1*A*).

qRT-PCR and Quantitation of Viral Genomes. Total RNA was extracted with the TRIzol reagent (Invitrogen) and used for first-strand cDNA synthesis with the ReverTra–Plus RT-PCR kit (Toyobo) according to the manufacturer's instruction. qPCR was performed with SYBR Green Realtime PCR Master Mix (Toyobo). The relative RNA amount was normalized to GAPDH. The specific primer sequences for each target gene are described in *SI Appendix*, Table S1. Each sample was done in triplicate (two independent experiments).

To measure the VSV viral genome in the organ tissues of infected mice, isolated organs were sliced into pieces. Total RNA was extracted with TRIzol reagent and subjected to qRT-PCR analyses with the specific primers as described in *SI Appendix*, Table S1. To measure the HSV viral genome, genomic DNA was isolated from the organ tissues of infected mice with Tianamp Genomic DNA kit (DP304-02; TianGen) and used for qPCR with the specific primers corresponding to the HSV ICP8 gene. The relative viral genomes were normalized to GAPDH and the specific primers are described in *SI Appendix*, Table S1.

Luciferase Assay. 293T cells were seeded on 12-well plates and transiently transfected with the luciferase reporter plasmid together with the expression plasmids or control plasmids using the Tenfect reagent (TEYE). As an internal control, *Renilla* reporter plasmid was transfected simultaneously. Luciferase assays were carried out in triplicate. Luciferase activity was measured 48 h post-transfection using the Dual-Luciferase Reporter Gene Assay kit (Beyotime Biotechnology) according to the manufacturer's instructions and normalized to *Renilla* activity. Each sample was done in triplicate (three independent experiments).

Confocal Microscopy. For the localization of PINLYP, MEF cells were grown on coverslips and transfected with the pLVX/mPINLYP-Flag plasmid. After 48-h transfection, cells were incubated with Mitotracker (red) for 30 min at 37 °C, washed with PBS for three times, and fixed in 4% paraformaldehyde for 15 min at room temperature. Cells were subsequently permeabilized with 50%/50% methanol/acetone for 20 min, stained with Flag antibody for mPINLYP, or MEFs were directly costained with Flag antibody for mPINLYP and calreticulin antibody for the ER, or GM130 antibody for Golgi, followed by detection with the secondary antibodies (Alexa-488 goat anti-mouse IgG for mPINLYP-Flag, and Alexa-568 donkey anti-rabbit IgG for calreticulin and GM130).

For the colocalization of PINLYP and TBK1, 293T cells were grown on coverslips and cotransfected with the pLVX/hPINLYP-Flag and pLVX/hTBK1-Myc plasmids. After 48-h transfection, cells were fixed, stained with the Flag and Myc antibodies, and detected with the secondary antibodies (Alexa-488 goat anti-mouse IgG for hPINLYP-Flag, Alexa-568 donkey anti-rabbit IgG for hTBK1-Myc). Cell nuclei were counterstained with DAPI. Images were acquired by using a confocal microscope (Olympus FV1200).

Immunoblotting, ELISA, and FACS. Immunoblot analyses were carried out with the specific antibodies as described in *SI Appendix*, Table S2. To measure the production of IFN-β by ELISA, culture supernatants were collected from the stimulated cells or serum samples were prepared from virus-infected mice. Detection of IFN-β was performed using a mouse IFN-β ELISA kit (PBL Biomedical Laboratories) according to the manufacturer's instructions. FACS analyses were performed using the specific antibodies as described in *SI Appendix*, Table S2.

Virus Tittering and Virus Infection in Mice. HSV-1 and VSV virus titers were measured using the 50% tissue culture infective dose ($TCID_{50}$) method as previously described (49). Titers were calculated as log($TCID_{50}$/mL) using the Spearman–Karber method. The titration was carried out in triplicate.

Age-matched, 7- to 8-wk-old (male and female) $PINLYP^{fl/fl}$ CD11c Cre- and $PINLYP^{fl/fl}$ CD11c Cre^{+} mice were intravenously injected with 1×10^8 pfu of HSV-1 or 5×10^8 pfu of VSV. The viability of the infected mice was monitored for 2 to 3 wk. Mouse sera were collected at 8 h postinfection to measure the serum IFN-β by ELISA as described above. To measure VSV viral genome, livers and spleens of the infected mice were collected and minced in TRIzol reagents for total RNA extraction and qRT-PCR. To measure the HSV-1 viral genome, brains and lungs of the infected mice were collected and minced in TIANamp Genomic DNA Kit (Tiangen) P1 buffer at 4 °C for genomic DNA isolation and qPCR.

Statistical Analysis. Statistical analyses were performed in Prism (Graph Pad Software). The data were reported as means ± SEM. Differences between groups of research subjects were analyzed for statistical significance with two-tailed unpaired *t* tests. Log-rank (Mantel-Cox) test was used to analyze the statistical significance of survival curves. A P value < 0.05 was considered significant. Statistical values were indicated in the figures by asterisks: $*P < 0.05$, $**P < 0.01$, $***P < 0.001$.

Data Availability. All study data are included in the main text and *SI Appendix*.

ACKNOWLEDGMENTS. We thank Prof. Jin Zhong (Institut Pasteur of Shanghai) for providing the pLVX/puromycin vector and Prof. Guangxun Meng (Institut Pasteur of Shanghai) for providing LysM cre mice. Support for this work was provided by the grants from the Ministry of Science and Technology of China (2016YFA0502100), the Natural Science Foundation of China (81871657), the Shanghai municipal science and technology key project: Research on core technologies for prevention and control of emerging infectious diseases, and the Open Project of the State Key Laboratory of Trauma, Burns, and Combined Injury (SKLKF201902).

1. E. V. Mesev, R. A. LeDesma, A. Ploss, Decoding type I and III interferon signalling during viral infection. *Nat. Microbiol.* **4**, 914–924 (2019).
2. H. M. Lazear, J. W. Schoggins, M. S. Diamond, Shared and distinct functions of type I and type III interferons. *Immunity* **50**, 907–923 (2019).
3. F. McNab, K. Mayer-Barber, A. Sher, A. Wack, A. O'Garra, Type I interferons in infectious disease. *Nat. Rev. Immunol.* **15**, 87–103 (2015).
4. P. J. Hertzog, B. R. Williams, Fine tuning type I interferon responses. *Cytokine Growth Factor Rev.* **24**, 217–225 (2013).
5. A. Isaacs, J. Lindenmann, Virus interference. I. The interferon. *Proc. R. Soc. Lond. B Biol. Sci.* **147**, 258–267 (1957).
6. A. Isaacs, J. Lindenmann, R. C. Valentine, Virus interference. II. Some properties of interferon. *Proc. R. Soc. Lond. B Biol. Sci.* **147**, 268–273 (1957).
7. F. J. Barrat, M. K. Crow, L. B. Ivashkiv, Interferon target-gene expression and epigenomic signatures in health and disease. *Nat. Immunol.* **20**, 1574–1583 (2019).
8. C. T. Ng, J. L. Mendoza, K. C. Garcia, M. B. Oldstone, Alpha and beta type 1 interferon signaling: Passage for diverse biologic outcomes. *Cell* **164**, 349–352 (2016).
9. K. Honda, H. Yanai, A. Takaoka, T. Taniguchi, Regulation of the type I IFN induction: A current view. *Int. Immunol.* **17**, 1367–1378 (2005).
10. A. Pichlmair, C. Reis e Sousa, Innate recognition of viruses. *Immunity* **27**, 370–383 (2007).
11. N. Yan, Z. J. Chen, Intrinsic antiviral immunity. *Nat. Immunol.* **13**, 214–222 (2012).
12. D. Walsh, J. McCarthy, C. O'Driscoll, S. Melgar, Pattern recognition receptors—Molecular orchestrators of inflammation in inflammatory bowel disease. *Cytokine Growth Factor Rev.* **24**, 91–104 (2013).
13. G. P. Amarante-Mendes *et al.*, Pattern recognition receptors and the host cell death molecular machinery. *Front. Immunol.* **9**, 2379 (2018).
14. M. R. Thompson, J. J. Kaminski, E. A. Kurt-Jones, K. A. Fitzgerald, Pattern recognition receptors and the innate immune response to viral infection. *Viruses* **3**, 920–940 (2011).
15. J. Wu, Z. J. Chen, Innate immune sensing and signaling of cytosolic nucleic acids. *Annu. Rev. Immunol.* **32**, 461–488 (2014).
16. T. Kawai, S. Akira, Toll-like receptors and their crosstalk with other innate receptors in infection and immunity. *Immunity* **34**, 637–650 (2011).
17. L. A. O'Neill, D. Golenbock, A. G. Bowie, The history of Toll-like receptors—Redefining innate immunity. *Nat. Rev. Immunol.* **13**, 453–460 (2013).
18. L. Sun, J. Wu, F. Du, X. Chen, Z. J. Chen, Cyclic GMP-AMP synthase is a cytosolic DNA sensor that activates the type I interferon pathway. *Science* **339**, 786–791 (2013).
19. J. Wu *et al.*, Cyclic GMP-AMP is an endogenous second messenger in innate immune signaling by cytosolic DNA. *Science* **339**, 826–830 (2013).
20. H. Ishikawa, Z. Ma, G. N. Barber, STING regulates intracellular DNA-mediated, type I interferon-dependent innate immunity. *Nature* **461**, 788–792 (2009).
21. X. Zhang *et al.*, Cyclic GMP-AMP containing mixed phosphodiester linkages is an endogenous high-affinity ligand for STING. *Mol. Cell* **51**, 226–235 (2013).
22. B. Zhong *et al.*, The adaptor protein MITA links virus-sensing receptors to IRF3 transcription factor activation. *Immunity* **29**, 538–550 (2008).
23. Q. Chen, L. Sun, Z. J. Chen, Regulation and function of the cGAS-STING pathway of cytosolic DNA sensing. *Nat. Immunol.* **17**, 1142–1149 (2016).
24. N. Dobbs *et al.*, STING activation by translocation from the ER is associated with infection and autoinflammatory disease. *Cell Host Microbe* **18**, 157–168 (2015).

25. M. Schlee, G. Hartmann, Discriminating self from non-self in nucleic acid sensing. *Nat. Rev. Immunol.* **16**, 566–580 (2016).
26. J. Rehwinkel, M. U. Gack, RIG-I-like receptors: Their regulation and roles in RNA sensing. *Nat. Rev. Immunol.* **20**, 537–551 (2020).
27. Y. M. Loo, M. Gale, Jr, Immune signaling by RIG-I-like receptors. *Immunity* **34**, 680–692 (2011).
28. C. L. Loughner *et al.*, Organization, evolution and functions of the human and mouse Ly6/uPAR family genes. *Hum. Genomics* **10**, 10 (2016).
29. X. Liang *et al.*, Murine gamma-herpesvirus immortalization of fetal liver-derived B cells requires both the viral cyclin D homolog and latency-associated nuclear antigen. *PLoS Pathog.* **7**, e1002220 (2011).
30. J. L. Pomerantz, D. Baltimore, NF-kappaB activation by a signaling complex containing TRAF2, TANK and TBK1, a novel IKK-related kinase. *EMBO J.* **18**, 6694–6704 (1999).
31. Y. Tojima *et al.*, NAK is an IkappaB kinase-activating kinase. *Nature* **404**, 778–782 (2000).
32. K. A. Fitzgerald *et al.*, IKKepsilon and TBK1 are essential components of the IRF3 signaling pathway. *Nat. Immunol.* **4**, 491–496 (2003).
33. S. Sharma *et al.*, Triggering the interferon antiviral response through an IKK-related pathway. *Science* **300**, 1148–1151 (2003).
34. W. Chen *et al.*, Contribution of Ser386 and Ser396 to activation of interferon regulatory factor 3. *J. Mol. Biol.* **379**, 251–260 (2008).
35. T. P. Gumley, I. F. McKenzie, M. S. Sandrin, Tissue expression, structure and function of the murine Ly-6 family of molecules. *Immunol. Cell Biol.* **73**, 277–296 (1995).
36. H. K. Kong, J. H. Park, Characterization and function of human Ly-6/uPAR molecules. *BMB Rep.* **45**, 595–603 (2012).
37. A. Davies *et al.*, CD59, an LY-6-like protein expressed in human lymphoid cells, regulates the action of the complement membrane attack complex on homologous cells. *J. Exp. Med.* **170**, 637–654 (1989).
38. H. W. Smith, C. J. Marshall, Regulation of cell signalling by uPAR. *Nat. Rev. Mol. Cell Biol.* **11**, 23–36 (2010).
39. F. Blasi, P. Carmeliet, uPAR: A versatile signalling orchestrator. *Nat. Rev. Mol. Cell Biol.* **3**, 932–943 (2002).
40. P. Y. Lee, J. X. Wang, E. Parisini, C. C. Dascher, P. A. Nigrovic, Ly6 family proteins in neutrophil biology. *J. Leukoc. Biol.* **94**, 585–594 (2013).
41. H. Wang *et al.*, Nicotinic acetylcholine receptor alpha7 subunit is an essential regulator of inflammation. *Nature* **421**, 384–388 (2003).
42. H. Ishikawa, G. N. Barber, STING is an endoplasmic reticulum adaptor that facilitates innate immune signalling. *Nature* **455**, 674–678 (2008).
43. E. Ogawa, K. Mukai, K. Saito, H. Arai, T. Taguchi, The binding of TBK1 to STING requires exocytic membrane traffic from the ER. *Biochem. Biophys. Res. Commun.* **503**, 138–145 (2018).
44. E. Helgason, Q. T. Phung, E. C. Dueber, Recent insights into the complexity of Tank-binding kinase 1 signaling networks: The emerging role of cellular localization in the activation and substrate specificity of TBK1. *FEBS Lett.* **587**, 1230–1237 (2013).
45. J. Yu, V. Murthy, S. L. Liu, Relating GPI-anchored Ly6 proteins uPAR and CD59 to viral infection. *Viruses* **11**, E1060 (2019).
46. S. B. Rasmussen *et al.*, Type I interferon production during herpes simplex virus infection is controlled by cell-type-specific viral recognition through Toll-like receptor 9, the mitochondrial antiviral signaling protein pathway, and novel recognition systems. *J. Virol.* **81**, 13315–13324 (2007).
47. S. Liu *et al.*, Interleukin 16 contributes to gammaherpesvirus pathogenesis by inhibiting viral reactivation. *PLoS Pathog.* **16**, e1008701 (2020).
48. C. Zhou *et al.*, Transfer of cGAMP into bystander cells via LRRC8 volume-regulated anion channels augments STING-mediated interferon responses and anti-viral immunity. *Immunity* **52**, 767–781.e6 (2020).
49. S. Liu, L. Li, L. Tan, X. Liang, Inhibition of herpes simplex virus-1 replication by natural compound honokiol. *Virol. Sin.* **34**, 315–323 (2019).